Journal of Materials Chemistry C

ROYAL SOCIETY OF CHEMISTRY

PAPER

View Article Online
View Journal | View Issue

Cite this: J. Mater. Chem. C, 2022, 10, 13262

Received 23rd June 2022,
Accepted 26th August 2022

DOI: 10.1039/d2tc02655d

rsc.li/materials-c

Luminescence quenching in epitaxially grown PCN-224 type metal–organic frameworks†

Tobias Burger,[a] Miriam de J. Velásquez-Hernández,[b] Robert Saf,[c] Sergey M. Borisov *[a] and Christian Slugovc *[c]

Core–shell and multivariant metal–organic frameworks (MOFs) of the PCN-224 type were prepared using metal-free and metalated porphyrin building blocks. Probing these MOFs with luminescence quenching upon exposure to oxygen reveals efficient gas transport and oxygen quenching in the core of the MOF. Undesirable energy transfer results in diminished contribution of the phosphorescent component in all mixed MOFs except for the physical mixture of individual crystals used as a reference.

Introduction

Luminescence quenching in some metal–organic frameworks (MOFs) is known to be very efficient, making these materials interesting candidates for application in optical oxygen sensors.[1] Particularly intriguing is the porphyrinic MOF class PCN-224, which is characterized by high porosity, and good stability in presence of acids, bases, organic solvents or at high temperature.[2] The PCN-224 MOFs are characterized by efficient absorption of visible light and variable luminescence decay times (nanoseconds to hundreds of microseconds) depending on the use of the free or differently metalated porphyrin linkers.[3] Accordingly, PCN-224-based materials show tunable dynamic ranges making them suitable for *e.g.* ultra-trace sensing of oxygen in the gas phase[3] or sensing of ambient oxygen concentrations in water.[4] Although such MOF-based oxygen sensor materials evolved as an interesting alternative to conventional polymer based sensors,[5] insights in their working principle are hardly available. We herein wish to contribute to a more comprehensive understanding of MOF-based optical sensors by tackling the question whether chromophores from the inner core of the crystal participate in the sensing event. The luminescence from the chromophores located in the core of the MOF might be limited or even completely undetectable due to possible absorption of the entire excitation light in the outer layer of the framework by "primary inner filter effect" and/or by reabsorption of the light emitted from the core by the outer layer ("secondary inner filter effect").[6] Moreover, luminescence quenching may be significantly less efficient due to lower accessibility of the inner parts of the crystal to oxygen. This information however is not only crucial for understanding of MOFs' function as optical sensor materials, but also as photocatalytic materials,[7] photosensitizers for photodynamic therapy[8] and in bioremediation applications.[9] We prepared core–shell MOFs (often referred to as MOF-on-MOF materials) with isostructural elements that utilize organic linkers with significantly different photophysical properties[10] and studied their different emission spectra and oxygen quenching behavior. PCN-224 type materials are supposedly well suited for this endeavor since differently metalated and free porphyrin ligands crystallize in the same space group with the same lattice constants.[1,2]

Results and discussion

The core–shell MOFs were prepared by a two-step procedure using 5,10,15,20-tetrakis-(4-carboxyphenyl)-21,23*H*-porphyrin (H_2TCPP) and its Pt(II) complex (Pt(II)TCPP) as the ligands. First, the core was synthesized by the conventional solvothermal reaction. In a second step, instead of isolating the crystals, the supernatant was exchanged for a solution of the other ligand. The solvothermal synthesis was then continued hoping for a fast crystal growth compared to nucleation of new crystals with the second ligand (see ESI† for details). The resulting crystalline materials were characterized by powder X-ray diffraction (pXRD) and optical microscopy as well as scanning electron microscopy. The ratio between H_2TCPP and Pt(II)TCPP incorporated into the

[a] Graz University of Technology, Institute of Analytical Chemistry and Food Chemistry, Stremayrgasse 9, 8010, Graz, Austria. E-mail: sergey.borisov@tugraz.at
[b] Graz University of Technology, Institute of Physical and Theoretical Chemistry, Stremayrgasse 9, 8010, Graz, Austria
[c] Graz University of Technology, Institute for Chemistry and Technology of Materials, Stremayrgasse 9, 8010, Graz, Austria. E-mail: slugovc@tugraz.at

† Electronic supplementary information (ESI) available: Experimental details and syntheses, optical and scanning electron micrographs, particle size distribution, information on the observed side product, UV-vis spectra from digestion experiments and Stern–Volmer plots. See DOI: https://doi.org/10.1039/d2tc02655d

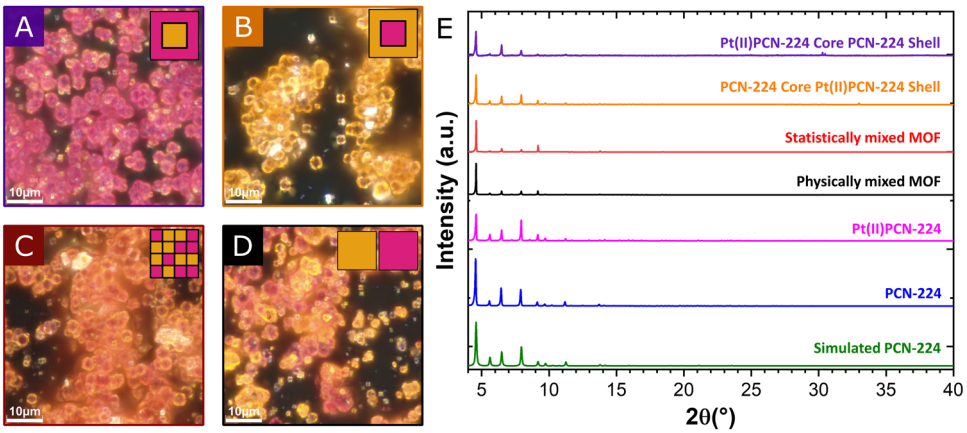

Fig. 1 Optical light microscopy images of the materials: (A) MOF with Pt(II)PCN-224 in the core and PCN-224 in the shell; (B) MOF with PCN-224 in the core and Pt(II)PCN-224 in the shell; (C) MOF with statistically mixed Pt(II)PCN-224 and PCN-224 parts and (D) physically mixed Pt(II)PCN-224 and PCN-224 crystals; (E) PXRD patterns for the same samples and reference materials.

core–shell materials was determined by digestion and quantification by UV/Vis spectroscopy.[11] Optical microscopy allows for identifying the respective shell materials by color. MOFs with Pt(II)PCN-224 core and PCN-224 shell appear as rosy crystals (Fig. 1A) similar to the pure PCN-224 MOF, whereas the MOF composed of PCN-224 core and Pt(II)PCN-224 shell is yellow (Fig. 1B). In addition to the core–shell materials, a multivariate MOF version[12] with putatively statistically distributed ligands was prepared by using a 1 : 1 mixture of H_2TCPP and Pt(II)TCPP during the synthesis. The statistically distributed MOF variant (Fig. 1C) is obtained as orange crystals, which suggests the formation of the intended MOF architecture. Although pXRD confirmed the phase purity of the core–shell MOF materials (Fig. 1E), some white material, supposedly an amorphous inorganic Zr containing compound (see ESI,† Fig. S9–S11 for discussion), has also been detected by optical microscopy. Further, a physical mixture of individually prepared PCN-224 and Pt(II)PCN-224 crystals serving as a reference was investigated. In optical microscopy, the physically mixed MOF sample appeared as two sorts of crystallites easily distinguishable by their color (Fig. 1D). Crystal sizes of all samples were found to be in the range of few micrometers and both crystal size and crystal size distributions were similar in every case (Fig. S1–S7, ESI†). This finding further supports the formation of the proposed core–shell structures, since the formation of novel crystallites consisting of mainly the second porphyrin (nucleation is fast) should increase the crystal size distribution.

Dissolution experiments of the respective MOF materials confirm the successful integration of both porphyrin ligands in the mixed MOFs (Fig. S12–S17, ESI†) and allow for the estimation of the PCN-224 and Pt(II)PCN-224 ratio (Table S1, ESI†). Three variants of the core–shell MOFs with Pt(II)TCPP in the core were prepared by growing the PCN-224 shell for 24 h, 48 h and 72 h leading to an increasing ratio of H_2TCPP from 1 : 1 to 1 : 5 (Table S1, ESI†). The MOF with statistically co-crystallized ligands has a Pt(II)TCPP to H_2TCPP ratio of 1 : 1.25, indicating faster incorporation of H_2TCPP into the crystal.

In the next step, the emission of the materials under defined oxygen partial pressures was measured using a previously reported measurement set-up.[3] As the excitation wavelength 410 nm was chosen in order to excite both chromophores in the MOF. Accordingly, the combined luminescence of Pt(II)PCN-224 and PCN-224 was recorded at 650 nm. The oxygen quenching behavior of the two individual MOFs is known. Pt(II)PCN-224 shows phosphorescence which is already quenched by traces of oxygen (pO_2 of 0.2 kPa). In contrast, PCN-224 exhibits fluorescence which is quenched around 4-fold at 20 kPa.[3] Therefore, by studying luminescence quenching under different ranges of oxygen partial pressure, the contribution of the respective material can be assessed. The quenching behavior of the physically mixed MOF crystals is illustrated in Fig. 2A. Under nitrogen atmosphere (1) the combined luminescence of PCN-224 and Pt(II)PCN-224 is observed. Under air (2) luminescence of both materials is efficiently quenched and only little residual fluorescence of PCN-224 is observed. Between (2) and (3) the luminescence of the more sensitive Pt(II)PCN-224 is still completely quenched and the observed decrease of luminescence intensity is fully due to quenching of PCN-224. Finally, the luminescence of both components is fully recovered after deoxygenation (4). The Stern–Volmer plots for the four different MOF samples are shown in Fig. 2B (individual Stern–Volmer plots are available as Fig. S18–S24, ESI†). The physically mixed MOF is characterized by a steep slope in the low pO_2 range that is associated with quenching of the Pt(II)PCN-224 luminescence and a moderate slope at higher pO_2 that originates from quenching of PCN-224. At low pO_2 values the behavior is thus very similar to that of the pure Pt(II)PCN-224 (Fig. 2B, inset).

The quenching behavior of all other MOFs is strikingly different (Fig. 2B, left) with the sensitivity much below that of the physically mixed MOF and similar to that of the pure PCN-224. We speculate that in all cases the major reason for this is the energy transfer from Pt(II)TCPP to H_2TCPP that strongly reduces the contribution of the phosphorescence of the former compared to what would be expected based on the ratio of both building blocks (Table S1, ESI†). Excitation spectra acquired for

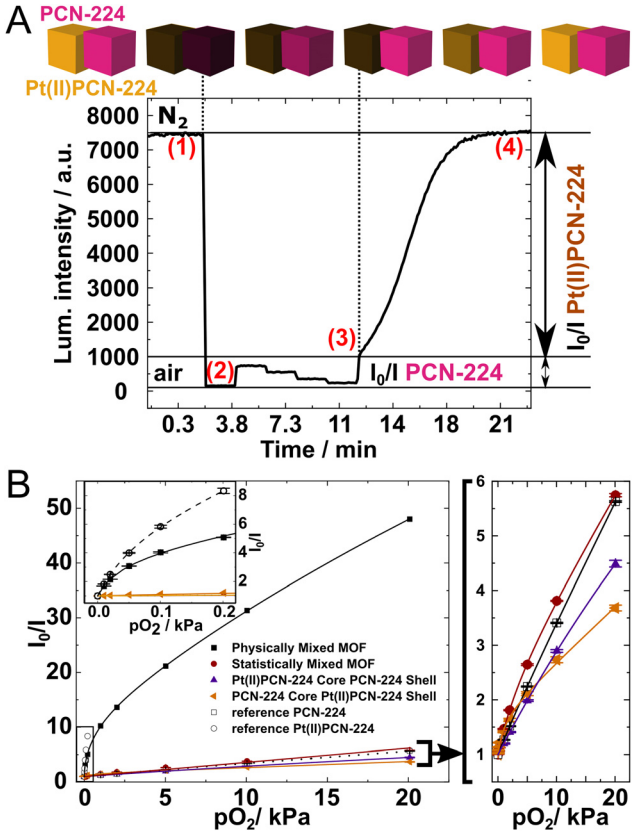

Fig. 2 (A) Dynamic response of the luminescence intensity *vs.* alteration of oxygen concentration for the physically mixed MOF composed of PCN-224 (purple) and Pt(II)PCN-224 (yellow); the color code of the cubes on top illustrates which of the two MOF is quenched; numbers (1) and (4) 0 kPa O_2; (2) 20 kPa O_2, steps between (2) and (3): 1 kPa, 2 kPa, 5 kPa, 10 kPa pO_2. (B) Stern–Volmer plots of the mixed MOFs; all calibrations were acquired at room temperature, λ_{Ex} = 410 nm, recorded at λ_{Em} = 650 nm; inset: magnification of the low pO_2 range; right panel – magnification for the materials showing less efficient quenching.

the physical mixture of the MOFs and the statistically mixed MOFs (Fig. S25 and S26, respectively, ESI†), confirm that in the latter the contribution of the phosphorescent Pt(II) porphyrin is significantly lower than expected. According to the crystal structure of PCN-224, the shortest distance of the porphyrins in a theoretically perfect PCN-224 crystal is around 14 Å. The distance separating two adjacent porphyrins is around 19 Å.[13a,b] The situation is similar for other porphyrinic MOF materials (PCN-223) for which Förster resonance transfer (FRET) was held responsible for the observed long-distance exciton hopping.[14] The spectral overlap between the emission of Pt(II)TCPP and the absorption of H_2TCPP (Fig. S27, ESI†) suggests that triplet-to-singlet FRET[13] from Pt(II)TCPP to H_2TCPP may be responsible for the decreased contribution of Pt(II)PCN-224 in the mixed MOFs. The Stern–Volmer plots (Fig. 2B) suggest that this effect is observed in all the MOFs where both dyes can be in the proximity. In case of the statistically mixed MOF more or less homogeneous distribution of both dyes is expected. On the other hand, the core–shell MOFs were expected to show spatial separation of both components and therefore quenching behavior similar to that of the physically mixed MOF. The major reason for the diminished contribution of Pt(II)PCN-224 in the core–shell MOFs is likely to be incorporation of some metal-free porphyrin into the Pt(II)PCN-224 core during the shell synthesis (in case of Pt(II)PCN-224 core-PCN-224 shell architecture) or partial dissolution of H_2TCPP from the core and its incorporation into the shell in case of the MOF with PCN-224 core-Pt(II)PCN-224 shell architecture. The luminescent behavior of the core–shell MOFs is thus in great contrast with their color (Fig. 1A–C) which corresponds to the color of the MOF that is predominately present in the shell.

Changing of the excitation wavelength from 410 nm to 500 nm results in an increased sensitivity to oxygen for the core–shell MOFs but also for the statistically mixed MOF (Fig. 3). This may be due to better penetration depth of the green light compared to the violet light. The highest increase in the sensitivity is observed for the MOF that consist of the Pt(II)PCN-224 core and thin PCN-224 shell. In this case the shell of PCN-224 is likely to significantly reduce the intensity of the violet light that reaches the Pt(II)PCN-224 core and much less so if the crystal is exposed to green light. In fact, the excitation wavelength of 410 nm corresponds to the Soret band of the porphyrin where molar absorption coefficient is particularly high (ε = 270 000 M^{-1} cm^{-1})[15] in contrast to much less intense Q-bands of the porphyrin that are located in the green part of the spectrum. The average edge length of the core–shell crystals after 24 h growth (Fig. 3B) is estimated to be 2.6 μm (see ESI† for more details) whereas the size of the core is about 1.4 μm. That gives the shell thickness of about 0.6 μm. Considering the density of the MOFs and absorption in aqueous solution it is estimated that about 50% of excitation light is absorbed by the shell if the excitation is performed around the Soret band (see ESI† for more details). For comparison, only 10% of the green light (500 nm) is expected to be absorbed by the same shell. It should be considered that the magnitude of the optical filtering is estimated for the monolayer of the MOFs which was not the case during the characterization experiments. Since the characterized powder sample consisted of several layers of MOF crystals, the above optical filtering effects are expected to be much more severe than calculated for the monolayer. Optical shielding by a shell of PCN-224 is expected to become more severe with increasing shell thickness, which was also observed in the experiment (Fig. 3B). In fact, the Stern–Volmer plots obtained at 410 and 500 nm excitation are now more similar with only a slight increase in sensitivity observed for 500 nm excitation. The edge length roughly doubles when it is grown for further 48 h and the shell thickness is estimated to be about 2 μm (Table S2, ESI†), which is roughly 3-times of the original thickness. An additional factor is the increased inner-filter effect due to reabsorption of the phosphorescence emitted from the Pt(II)PCN-224 core by the PCN-224 shell. Despite these complications, one can conclude that the core of the mixed MOF is accessible for oxygen and quenching of luminescence by this gas also occurs in the inner part of the MOF.

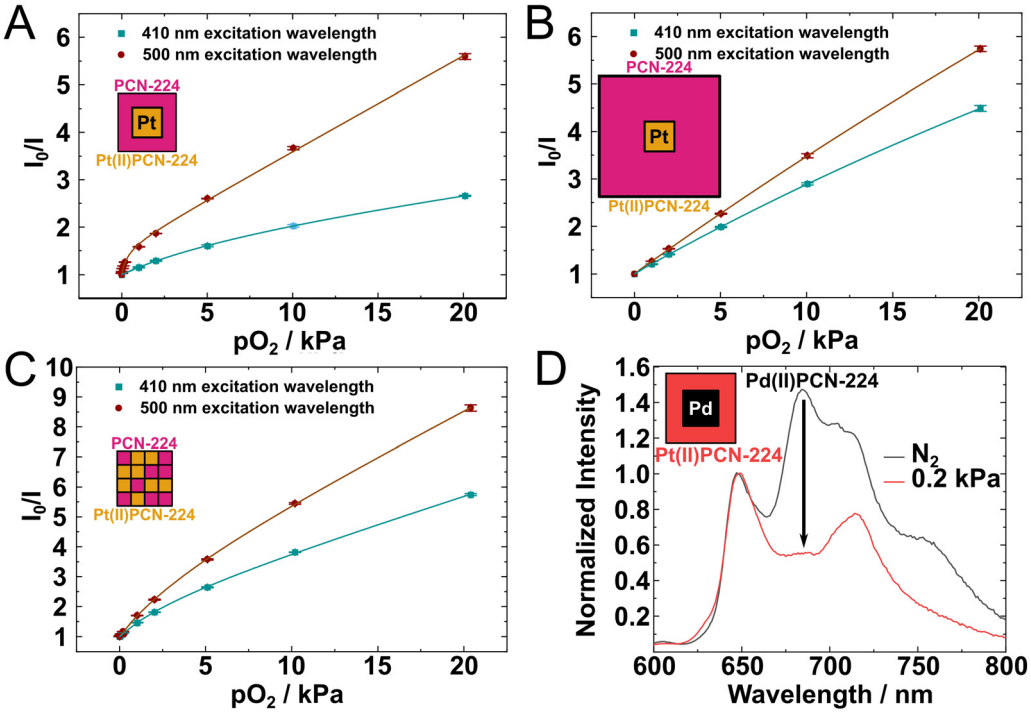

Fig. 3 Stern–Volmer plot for the MOF materials with λ_{Ex} = 410 nm and λ_{Ex} = 500 nm, λ_{Em} = 650 nm: (A) Pt(II)PCN-224 in the core and PCN-224 in the shell, 24 h of shell growth; (B) Pt(II)PCN-224 in the core and PCN-224 in the shell after 72 h of shell growth; (C) Pt(II)PCN-224 and PCN-224 statistically distributed; (D) emission spectra of the core shell MOF with Pd(II)PCN-224 in the core and Pt(II)PCN-224 in the shell, normalized to the emission of Pt(II)PCN-224 (650 nm); λ_{Ex} = 410 nm.

It should be mentioned that fitting of the Stern–Volmer plots with pronounced contribution from Pt(II)PCN-224 becomes challenging. The physically mixed MOF sample is a good example of the limitation of established Stern–Volmer fit models, *i.e.* the classical Stern–Volmer equation (eqn (S1), ESI†) or the non-linear equation from the so called "two-site model"[16] (eqn (S2), ESI†) that assumes the location of the indicator in two environments characterized by significantly different oxygen accessibility. Since the one component MOFs already show significant nonlinearity in their Stern–Volmer plots,[3] a further extension of the model is necessary. Although the best fit (R^2 = 0.99999) is obtained with the model assuming 4 different Stern–Volmer constants, the complexity of such a model is very high. The model assuming 3 different K_{SV} values also excellently fits the experimental data (R^2 = 0.9999) and appears to be a good compromise (see ESI† for details).

Finally, MOFs with Pd(II)PCN-224 and Pt(II)PCN-224 structures in the core and in the shell were prepared (Fig. S32–S34, ESI†). Since the absorption bands of both dyes are located in the green part of the electromagnetic spectrum and the emission in the red part, neither the inner-filter effect nor FRET is expected for this MOF combination. Due to longer phosphorescence decay time of the palladium porphyrin, Pd(II)PCN-224 is more sensitive to oxygen than Pt(II)PCN-224 and responds in the ultra-low range (0–20 ppm) in gas phase.[3]

Emission wavelengths of Pt(II)PCN-224 and Pd(II)PCN-224 are well separated from each other (650 nm and 680 nm, respectively), allowing simultaneous readout with the same excitation wavelength. Calibration of ultra-trace sensing materials is challenging, thus only emission spectra in oxygen-free atmosphere and at 0.2 kPa pO_2 were recorded (Fig. 3D). The emission of Pd(II)PCN-224 at around 680 nm can be observed in both core–shell MOFs under oxygen-free conditions and is strongly quenched at already 0.2 kPa pO_2. Unfortunately, Pd(II)PCN-224 is prone to partial demetalation under elevated temperatures and acidic conditions[17] so that the core–shell MOFs show additional spectral features attributed to emission from PCN-224 (Fig. 3D and Fig. S35, S36, ESI†). The impurity of the PCN-224 in the Pd(II)PCN-224 shell might promote undesired effects discussed above for the other mixed MOFs. For the MOF composed of Pd(II)PCN-224 core and Pt(II)PCN-224 shell the amount of PCN-224 impurities is lower than in the material with Pd(II)PCN-224 in the shell that suggests a protective effect of the shell in such materials. This concludes that such mixed MOFs should be constructed in a way that the more vulnerable components are located in the core and are thus protected by the shell. As the main point, data clearly show the quenching of the luminescence of the core material.

Conclusion

Altogether, we could experimentally show that the core of the mixed MOFs of the PCN-224 type is accessible for oxygen as quenching of luminescence also occurs in the inner part of the MOF.

The photophysical properties of the mixed MOF crystals investigated here are dominated by the high concentration of porphyrin building blocks and their proximity. Energy transfer is likely to play a pivotal role in reducing the contribution of the phosphorescent component in the mixed MOFs. Furthermore, optical filtering of the excitation light by the shell is of fundamental importance, the same is true for reabsorption of light emitted by the core. Since the magnitude of these effects is proportional to the thickness of the shell, the size of crystals is of major importance. The amount of the excitation light reaching the core of the crystal also depends on the excitation wavelength.

Apart from the insights on the photoactivity of core–shell materials, the physical mixture of individually prepared PCN-224 and Pt(II)PCN-224 crystals allows to profit from their individual outstanding sensing properties and to obtain sensors covering the range from trace oxygen amount to air-saturated conditions or even 100% O_2. For such applications, the physical mixture of MOF crystals is found to be superior to any mixture of the building blocks within a single crystal.

Author contributions

T. B. performed most experiments, analyzed the data and prepared the initial draft of the manuscript. M. V.-H. performed structural characterization, R. S. provided optical micrographs, C. S. and S. B. conceived, supervised and directed the study and acquired the funding. All authors contributed to the analysis of the results and to the writing of the manuscript.

Conflicts of interest

The authors have no conflicts of interest to declare.

Acknowledgements

The work was financially supported by the Graz University of Technology through the lead-project LP-03 (Porous Materials at Work). We acknowledge Paolo Falcaro for the free access to the X-ray facility and Fernando Gustavo Warchomicka for providing SEM and EDX analyses.

References

1 (*a*) R.-B. Lin, F. Li, S.-Y. Liu, X.-L. Qi, J.-P. Zhang and X.-M. Chen, A Noble-Metal-Free Porous Coordination Framework with Exceptional Sensing Efficiency for Oxygen, *Angew. Chem., Int. Ed.*, 2013, **52**, 13429–13433, DOI: **10.1002/anie.201307217**; (*b*) S.-Y. Liu, X.-L. Qi, R.-B. Lin, X.-N. Cheng, P.-Q. Liao, J.-P. Zhang and X.-M. Chen, Porous Cu(I) Triazolate Framework and Derived Hybrid Membrane with Exceptionally High Sensing Efficiency for Gaseous Oxygen, *Adv. Funct. Mater.*, 2014, **24**, 5866–5872, DOI: **10.1002/adfm.201401125**; (*c*) S.-Y. Liu, D.-D. Zhou, C.-T. He, P.-Q. Liao, X.-N. Cheng, Y.-T. Xu, J.-W. Ye, J.-P. Zhang and X.-M. Chen, Flexible, Luminescent Metal–Organic Frameworks Showing Synergistic Solid-Solution Effects on Porosity and Sensitivity, *Angew. Chem., Int. Ed.*, 2016, **55**, 16021–16025, DOI: **10.1002/anie.201608439**.

2 (*a*) D. Feng, W.-C. Chung, Z. Wei, Z.-Y. Gu, H.-L. Jiang, Y.-P. Chen, D. J. Darensbourg and H.-C. Zhou, Construction of Ultrastable Porphyrin Zr Metal–Organic Frameworks through Linker Elimination, *J. Am. Chem. Soc.*, 2013, **135**, 17105–17110, DOI: **10.1021/ja408084j**; (*b*) J. Wang, Y. Fan, Y. Tan, X. Zhao, Y. Zhang, C. Cheng and M. Yang, Porphyrinic Metal–Organic Framework PCN-224 Nanoparticles for Near-Infrared-Induced Attenuation of Aggregation and Neurotoxicity of Alzheimer's Amyloid-β Peptide, *ACS Appl. Mater. Interfaces*, 2018, **10**, 36615–36621, DOI: **10.1021/acsami.8b15452**.

3 T. Burger, C. Winkler, I. Dalfen, C. Slugovc and S. M. Borisov, Porphyrin based metal–organic frameworks: highly sensitive materials for optical sensing of oxygen in gas phase, *J. Mater. Chem. C*, 2021, **9**, 17099–17112, DOI: **10.1039/D1TC03735H**.

4 (*a*) J. Yang, Z. Wang, Y. Li, Q. Zhuang and J. Gu, Real-Time Monitoring of Dissolved Oxygen with Inherent Oxygen-Sensitive Centers in Metal–Organic Frameworks, *Chem. Mater.*, 2016, **28**, 2652–2658, DOI: **10.1021/acs.chemmater.6b00016**; (*b*) J. Yang, Z. Wang, Y. Li, Q. Zhuang, W. Zhao and J. Gu, Porphyrinic MOFs for reversible fluorescent and colorimetric sensing of mercury(ii) ions in aqueous phase, *RSC Adv.*, 2016, **6**, 69807–69814, DOI: **10.1039/C6RA13766K**.

5 I. Dalfen and S. M. Borisov, Porous matrix materials in optical sensing of gaseous oxygen, *Anal. Bioanal. Chem.*, 2022, **414**, 4311–4330, DOI: **10.1007/s00216-022-04014-6**.

6 (*a*) C. A. Parker and W. T. Rees, Fluorescence spectrometry. A review, *Analyst*, 1962, **87**, 83–111, DOI: **10.1039/AN9628700083**; (*b*) M. Kubista, R. Sjöback, S. Eriksson and B. Albinsson, Experimental correction for the inner-filter effect in fluorescence spectra, *Analyst*, 1994, **119**, 417–419, DOI: **10.1039/AN9941900417**.

7 (*a*) Y. Zong, S. Ma, J. Gao, M. Xu, J. Xue and M. Wang, Synthesis of Porphyrin Zr-MOFs for the Adsorption and Photodegradation of Antibiotics under Visible Light, *ACS Omega*, 2021, **6**, 17228–17238, DOI: **10.1021/acsomega.1c00919**; (*b*) L. Shi, L. Yang, H. Zhang, K. Chang, G. Zhao, T. Kako and J. Ye, Implantation of Iron(III) in porphyrinic metal organic frameworks for highly improved photocatalytic performance, *Appl. Catal., B*, 2018, **224**, 60–68, DOI: **10.1016/j.apcatb.2017.10.033**; (*c*) J. He, Y. Zhang, J. He, X. Zeng, X. Hou and Z. Long, Enhancement of photoredox catalytic properties of porphyrinic metal–organic frameworks based on titanium incorporation via post-synthetic modification, *Chem. Commun.*, 2018, **54**, 8610–8613, DOI: **10.1039/C8CC04891F**.

8 (*a*) J. Park, Q. Jiang, D. Feng, L. Mao and H.-C. Zhou, Size-Controlled Synthesis of Porphyrinic Metal–Organic Framework and Functionalization for Targeted Photodynamic Therapy, *J. Am. Chem. Soc.*, 2016, **138**, 3518–3525, DOI: **10.1021/jacs.6b00007**; (*b*) S.-S. Wan, J.-Y. Zeng, H. Cheng and X.-Z. Zhang, ROS-induced NO generation for gas therapy and sensitizing photodynamic therapy of tumor, *Biomaterials*, 2018,

185, 51–62, DOI: 10.1016/j.biomaterials.2018.09.004; (*c*) J.-Y. Zeng, M.-Z. Zou, M. Zhang, X.-S. Wang, X. Zeng, H. Cong and X.-Z. Zhang, π-Extended Benzoporphyrin-Based Metal–Organic Framework for Inhibition of Tumor Metastasis, *ACS Nano*, 2018, **12**, 4630–4640, DOI: 10.1021/acsnano.8b01186.

9 (*a*) P. D. Harvey, Porphyrin-based MOFs as heterogeneous photocatalysts for the eradication of organic pollutants and toxins, *J. Porphyrins Phthalocyanines*, 2021, **25**, 583–604, DOI: 10.1142/S1088424621300020; (*b*) D. Lin, X. Liu, R. Huang, W. Qi, R. Su and Z. He, One-pot synthesis of mercapto functionalized Zr-MOFs for the enhanced removal of Hg2+ ions from water, *Chem. Commun.*, 2019, **55**, 6775–6778, DOI: 10.1039/C9CC03481A.

10 (*a*) H.-Q. Yin and X.-B. Yin, Metal-Organic Frameworks with Multiple Luminescence Emissions: Design and Applications, *Acc. Chem. Res.*, 2020, **53**, 485–495, DOI: 10.1021/acs.accounts.9b00575; (*b*) W. J. Newsome, S. Ayad, J. Cordova, E. W. Reinheimer, A. D. Campiglia, J. K. Harper, K. Hanson and F. J. Uribe-Romo, Solid State Multicolor Emission in Substitutional Solid Solutions of Metal–Organic Frameworks, *J. Am. Chem. Soc.*, 2019, **141**, 11298–11303, DOI: 10.1021/jacs.9b05191; (*c*) N. Patel, P. Shukla, P. Lama, S. Das and T. K. Pal, Engineering of Metal–Organic Frameworks as Ratiometric Sensors, *Cryst. Growth Des.*, 2022, **22**, 3518–3564, DOI: 10.1021/acs.cgd.1c01268.

11 J. Chu, F.-S. Ke, Y. Wang, X. Feng, W. Chen, X. Ai, H. Yang and Y. Cao, Facile and reversible digestion and regeneration of zirconium-based metal-organic frameworks, *Commun. Chem.*, 2020, **3**, 5, DOI: 10.1038/s42004-019-0248-7.

12 H. Deng, C. J. Doonan, H. Furukawa, R. B. Ferreira, J. Towne, C. B. Knobler, B. Wang and O. M. Yaghi, Multiple Functional Groups of Varying Ratios in Metal-Organic Frameworks, *Science*, 2010, **327**, 846–850, DOI: 10.1126/science.1181761.

13 (*a*) Y.-Y. Liu, L.-J. Chen, X. Zhao and X.-P. Yan, Effect of Topology on Photodynamic Sterilization of Porphyrinic Metal-Organic Frameworks, *Chem. – Eur. J.*, 2021, **27**, 10151–10159, DOI: 10.1002/chem.202100920; (*b*) A. Cravcenco, M. Hertzog, C. Ye, M. N. Iqbal, U. Mueller, L. Eriksson and K. Börjesson, Multiplicity conversion based on intramolecular triplet-to-singlet energy transfer, *Sci. Adv.*, 2019, **5**, eaaw5978, DOI: 10.1126/sciadv.aaw5978.

14 S. M. Shaikh, A. Chakraborty, J. Alatis, M. Cai, E. Danilov and A. J. Morris, Light harvesting and energy transfer in a porphyrin-based metal organic framework, *Faraday Discuss.*, 2019, **216**, 174–190, DOI: 10.1039/C8FD00194D.

15 S. P. Hill, T. Dilbeck, E. Baduell and K. Hanson, Integrated Photon Upconversion Solar Cell via Molecular Self-Assembled Bilayers, *ACS Energy Lett.*, 2016, **1**, 3–8, DOI: 10.1021/acsenergylett.6b00001.

16 E. R. Carraway, J. N. Demas, B. A. DeGraff and J. R. Bacon, Photophysics and photochemistry of oxygen sensors based on luminescent transition-metal complexes, *Anal. Chem.*, 1991, **63**, 337–342, DOI: 10.1021/ac00004a007.

17 M. Speckbacher, L. Yu and J. S. Lindsey, Formation of Porphyrins in the Presence of Acid-Labile Metalloporphyrins: A New Route to Mixed-Metal Multiporphyrin Arrays, *Inorg. Chem.*, 2003, **42**, 4322–4337, DOI: 10.1021/ic026206d.